Anisotropic Encapsulation-Induced Synthesis of Asymmetric Single-Hole Mesoporous Nanocages

Xiaomin Li[†], Lei Zhou[†], Yong Wei[†], Ahmed Mohamed El-Toni[‡ §], Fan Zhang[†*], Dongyuan Zhao[†*]

†Department of Chemistry and Laboratory of Advanced Materials, State Key Laboratory of Molecular Engineering of Polymers, Collaborative Innovation Center of Chemistry for Energy Materials, Fudan University, Shanghai 200433, P. R. China.

[‡]King Abdullah Institute for Nanotechnology, King Saud University, Riyadh 11451, Saudi Arabia

[§]Central Metallurgical Research and Development Institute, CMRDI, Helwan 11421, Cairo, Egypt

[*] To whom correspondence should be addressed.

E-mail: zhang_fan@fudan.edu.cn; dyzhao@fudan.edu.cn

Supporting Information:

1. Materials.

Gadolinium (III) chloride anhydrous (**$GdCl_3$**, 99.99 %), ytterbium (III) chloride anhydrous ($YbCl_3$, 99.9 %), thulium (III) chloride anhydrous ($TmCl_3$, 99.9 %), cadmium oxide (CdO, 99.99 %), zinc oxide (ZnO, 99.99 %), selenium powder (Se, 99.99 %), iron(III) acetylacetonate [$Fe(acac)_3$, 99.9 %], Polyoxyethylene(5) Nonylphenyl Ether (IGEPAL CO-520), sodium trifluoroacetate (Na-TFA, 98 %), 1-octadecene (ODE, 90 %), oleic acid (OA, 90 %), hexadecyltrimethylammonium bromide (CTAB, 99 %), were purchased from Sigma-Aldrich. Sodium hydroxide (NaOH, 96 %), ammonium fluoride (NH_4F, 96 %), ethanol, 1-Octanol (99 %), trixton X-100 (98 %), NH_4NO_3 was obtained from Beijing Chemical Reagents Co. Ltd. Ammonia aqueous solution (28 wt %), tetraethylorthosilicate (TEOS, 99.9 %), doxorubicin hydrochloride (DOX, 98 %), albumin from bovine serum (BSA, 96 %) were purchased from Aladdin Industrial Inc. Bis(triethoxysilyl)ethane (BTEE) were purchased from Gelest Inc. All chemicals were used as received without any further purification.

2. Synthesis of dense SiO_2 seed nanoparticles.

The dense SiO_2 spherical nanoparticles were synthesized by using the reverse micro-emulsion method. Typically, 16.8 mL of 1-otcanol and 30 mL of trixton X-100 were dispersed in 120 mL of cyclohexane by sonication and stirring. Then, 1.0 mL of (28 wt %) ammonium hydroxide was added to form a reverse micro-emulsion solution. After stirring for 30 min, 0.8 mL of TEOS was added, and the reaction was

aged for 6 ~ 16 h (different sized nanoparticles could be obtained at different reaction time) under stirring. The final products were collected by centrifuging and washed by water and ethanol for several times. The dense SiO_2 nanoparticles were finally dispersed in 40 mL of water for the further use. For the synthesis of the dense SiO_2 nanoparticles with a size of ~ 35 nm, CO-520 was used as an emulsifying instead of 1-otcanol and trixton X-100.

3. Synthesis of NC@SiO_2 seed nanoparticles.

The syntheses of $NaGdF_4$:Yb,Tm@$NaGdF_4$ upconversion nanoparticles (UCNPs), CdSe@CdS@ZnS quantum dots (QDs), Fe_3O_4 inorganic functional nanocrystals in this work were similar to the procedures reported previously.[1-3] The NC@SiO_2 (NC = Nanocrystal: $NaGdF_4$:Yb,Tm@$NaGdF_4$ UCNP, CdSe@CdS@ZnS QD and Fe_3O_4 nanoparticle) were synthesized by using the reverse micro-emulsion method.[1-3] Taking the synthesis of UCNP@SiO_2 as an example, firstly, 4.2 mL of 1-otcanol and 7.5 mL of trixton X-100 were dispersed in 30 mL of cyclohexane by sonication and stirring. Then, 0.6 mL of the UCNPs cyclohexane solution obtained above (concentration of 10 mg/mL) was added into the above mixture. The resultant solution was stirred for 15 min, and then 0.26 mL of 28 wt% $NH_3 \cdot H_2O$ solution was added to form a reverse micro-emulsion solution. After stirring for 30 min, 0.2 mL of TEOS was added, and the reaction was aged for 16 h under stirring. The final product was collected by centrifuging and washed by water and ethanol for several times. The UCNP@SiO_2 nanoparticles were finally dispersed in 5 mL of water for the further use. The fabrication of the QDs@SiO_2 and Fe_3O_4@SiO_2 was similar with that of the above

UCNP@SiO_2 core-shell nanoparticles except CO-520 was used as an emulsifying.

4. Synthesis of eccentric single-hole mesoporous silica nanocages.

Typically, 5.0 mL of the dense SiO_2 nanoparticles solution prepared above was added into the solution containing 70 mL of water, 5.0 mL of ethanol, 150 mg of CTAB and 1.8 mL of ammonia aqueous solution (28 wt %). The mixture was turned to homo-dispersed solution after stirring for 30 min. Then, 0.4 mL of BTEE was added dropwise with continuous stirring and the reaction proceeded for 3 h. The particles were collected by centrifugation, washed with ethanol and water and dispersed in 50 mL of water. After the dense SiO_2 cores were etched by the hydrothermal process at 60 °C for 12 h, the eccentric hollow structure nanoparticles were obtained. Then, the eccentric hollow nanoparticles were dispersed in 120 mL of HF solution (0.2 ~ 0.5 %) for 30 min. Finally, the single-hole mesoporous silica nanocages with different hole sizes could be obtained (Figure S7).

5. Synthesis of eccentric single-hole UCNP@MSN nanorattles.

Typically, 5.0 mL of the UCNP@SiO_2 nanoparticles solution prepared above was added into the solution containing 70 mL of water, 5.0 mL of ethanol, 150 mg of CTAB and 1.8 mL of ammonia aqueous solution (28 wt %). The mixture was turned to homo-dispersed solution after stirring for 30 min. Then, 0.2 mL of BTEE was added dropwise with continuous stirring and the reaction was proceeded for 3 h. The particles were collected by centrifugation, washed with ethanol and water and dispersed in 50 mL of water. The SiO_2 layer was etched by the hydrothermal process at 60 °C for 12 h. Then, the eccentric hollow nanoparticles were dispersed in 120 mL

of (0.2 ~ 0.5 %) HF solution for 30 min. Finally, the eccentric single-hole UCNP@MSN nanorattles with different hole-sizes could be obtained.

6. Synthesis Azo-modified eccentric single-hole UCNP@MSN nanorattles.

The Azo-modified eccentric single-hole UCNP@MSN nanorattles were synthesized by using the post-modification method. Typically, the eccentric single-hole UCNP@MSN nanorattles were dispersed in the toluene solution of Azo coupled isocyanatopropylethoxysilane [4] and refluxed at 110 °C for 48 h. The particles were collected by centrifugation, washed with ethanol.

7. The fabrication of the guest delivery system.

The eccentric single-hole mesoporous silica nanocages could provide dual independent storage spaces for guest molecules. One was the hollow cave for large guest molecules, another was the mesopores in the shells for small guest molecules. Therefore, we selected two commonly used molecules with quite different sizes, DOX (< 1 nm^3) and BSA (21 × 4 × 14 nm^3), as model guests to evaluate the potentials of eccentric single-hole mesoporous silica nanocages for the novel guest delivery system. The main storage space for small DOX molecules was the mesopores in the shells. Although DOX molecules could also be loaded in the hollow cave, it could easily be leaked out from the hollow cave during the post washing step because the size of the hole was much larger than the diameter of DOX molecule. In contrast, the DOX molecules loaded in the mesoporous networks in the shells were more stable than in the hollow cave due to the relative smaller pore size of the mesopores in the shells. On the other hand, Azo switch molecules could also be used to lock DOX in the

mesopores of the shells. For the big BSA molecule, it had no alternative to be loaded in the hollow cave. Compared with the residues DOX molecules in the cave, BSA molecules were more difficult leaked out from the hollow cave during the post washing step because the diameter of BSA was much larger than DOX.

8. Adsorption of DOX.

Doxorubicin hydrochloride (10 mg) was dissolved in water (2.0 mL). Azo-modified eccentric single-hole UCNP@MSN nanorattles (5.0 mg) were added to the solution and the suspension was stirred at room temperature for 48 h. The DOX molecules could be adsorbed in the mesopore channels in the shells and locked by the Azo switch. In addition, the loading process of the DOX in the mesopore channels could be accelerated with the alternatively radiation of the UV and Vis light due to the rotation-inversion movement of the Azo molecules. The as-prepared DOX-loaded eccentric single-hole UCNP@MSN-Azo nanorattles were collected by centrifugation. The residues DOX molecules in the hollow could be easily washed off with water due to the presence of the big hole. The amount of the adsorbed guests was determined from the difference between the starting amount of DOX by measuring the absorbance of the drug from the supernatant liquid at 480 nm quantified from a standard curve.

9. Adsorption of BSA.

For loading of big BSA molecules, it had no alternative to be loaded in the hollow cave. BSA (20 mg) was dissolved in water (2.0 mL) and the DOX-loaded single-hole UCNP@MSN-Azo nanorattles were added with stirring at room temperature for 48 h.

Because of the presence of the big hole in the shells, the BSA molecules were easily adsorbed into the hollow voids of the nanocomposites. The as-prepared DOX and BSA co-loaded single-hole UCNP@MSN-Azo nanorattles were collected by centrifugation. The residues BSA molecules were washed off with water.

10. The modification of 1-tetradecanol phase changed material on the UCNP@MSN-Azo surface.

The DOX and BSA co-loaded single-hole UCNP@MSN-Azo nanorattles (5.0 mg) were dispersed in ethanol (2.0 mL) and 1-tetradecanol (2.5 mg) was added with stirring at room temperature for 30 min. Then, ethanol solvent was removed under vacuum condition. Finally, the DOX and BSA co-loaded single-hole UCNP@MSN-Azo-PCM nanorattles in powder were collected for the further use.

11. Heat and NIR light triggered release of BSA and DOX.

The schematic illustration of heat and NIR bimodal triggered BSA and DOX release experiments is shown in Figure S16. Typically, the mixture of the DOX, BSA co-loaded single-hole UCNP@MSN-Azo-PCM nanorattles (5.0 mg) and DI water (5.0 mL) was put on a heat plate (or conditioning oven) to control the temperature of the solution. An external NIR laser (980 nm, 5 W/cm^2) was introduced to irradiate the drug carrier.

12. Cytotoxicity of the single-hole mesoporous nanocages.

The cytotoxicity was measured by using the Cell Counting Kit-8 (CCK-8) assay in HeLa cell. The cells (1×10^4) were incubated in each well of a 96-well plate at 37 °C under 5 % CO_2 for 24 h. Then cells were incubated and cultured with the eccentric

single-hole mesoporous silica nanocages at different concentrations (10, 20, 50, 100 μg/mL) at 37 °C under 5 % CO_2 for another 24 h. Finally, 10 μL/well of CCK-8 in PBS solution was added to each well and incubated at 37 °C for 4 h. The quantity was determined calorimetrically by using a multi reader (TECAN, Infinite M200). The measurements were based on the absorbance values at 450 nm. The following formula was used to calculate the viability of cell growth: Viability (%) = (mean of absorbance value of treatment group/mean absorbance value of control) × 100.

13. Characterization

Transmission electron microscopy (TEM), high-resolution transmission electron microscopy (HRTEM), high-angle annular dark field imaging in the scanning TEM (HAADF-STEM) observations were performed on JEM-2100F transmission electron microscope with an accelerating voltage of 200 kV equipped with a post-column Gatan imaging filter (GIF-Tri-dium). Scanning electron microscopy (SEM) images were taken using a Hitachi S-4800 ultrahigh resolution cold FEG with an in-lens electron optic operating at 20 kV. The upconversion luminescence emission spectra were recorded on Hitachi Fluorescence Spectrometer F4500 instrument, but the excitation source using an external semiconductor laser (980 nm, Changchun New Industries Optoelectronics Tech. Co., Ltd.) with an optic fiber accessory, instead of the Xeon source in the spectrophotometer (Unless otherwise specified, all spectra were collected under identical experimental conditions). The UV/Vis spectra were recorded on Lambda 35 PerkinElmer. The measurements were conducted at 77 K with ASAP 2420 and Micromeritcs Tristar 3020 analyzer (USA). Before measurements,

the samples were degassed in vacuum at 120 °C for at least 12 h. Small-angle X-ray scattering (SAXS) measurements were taken on a Nanostar U small1angle X-ray scattering system (Bruker, Germany) using Cu Kα radiation (40 kV, 35 mA). The *d*-spacing values were calculated by the formula $d = 2\pi/q$, wherein q is the scattering vector.

14. The anisotropic nucleation, growth and encapsulation of PMO on the dense SiO_2 nanospheres

Due to the distinct chemical properties between TEOS and BTEE, the latter silica precursor with the hydrophobic organic group (-CH_2-CH_2-) leans toward anisotropic polymerization on the hydrophilic surface of the dense SiO_2 seeds through a heterogeneous nucleation process. As a result, the surface energy of the representative organic–inorganic hybrid structure PMO ($\sigma_{PMO\text{-}Solvent}$) in the H_2O/ethanol solvent increases as the volume percentage of H_2O increases. In contrast, the surface energy of the dense SiO_2 ($\sigma_{SiO2\text{-}Solvent}$) decreases as the volume percentage of H_2O increases. In our synthesis (H_2O/ethanol = 15 : 1), after the nucleation sites are formed, the negative total surface energy variation ($\Delta\sigma = \sigma_{PMO\text{-}Solvent} + \sigma_{PMO\text{-}SiO2} - \sigma_{SiO2\text{-}Solvent} < 0$) and the cubic symmetry mesostructure of the hydrophobic PMO domains can further induce anisotropic polymerization and the formation of the Janus nanostructure, meaning that the CTAB/silicate micelles are difficult to spread on the surface of dense SiO_2.[5-8] So, the energy barrier of the growth of PMO domain in the heterogeneous direction (*i.e.* dense SiO_2 direction) is much higher than that in the homogeneous directions (opposite to the hydrophilic dense SiO_2 direction), which induces the anisotropic growth of the initial PMO nucleus.[8] Through this anisotropic growth, the

PMO crystal nanoparticles can be formed and attached on the spherical dense SiO_2 seeds to realize the asymmetric nanocomposites. The "lattices" mismatch between the dense SiO_2 (non-porous) and PMO (cubic symmetry mesostructure) can induce the formation of disordered defect region at the hetero-interface. The growth of this disordered region is synchronized with the ordered cubic mesostructured region. Owing to the presence of great amount of disordered mesostructural defects, the morphology of the PMO domains were transferred from cube to the near-spherical, for further lowering the interface tension. Therefore, the whole dense SiO_2 nanosphere can be covered by the near-spherical PMO shells, the nanocomposites are transferred from the Janus nanoparticles to the near-spherical eccentric core@shell nanoparticles.

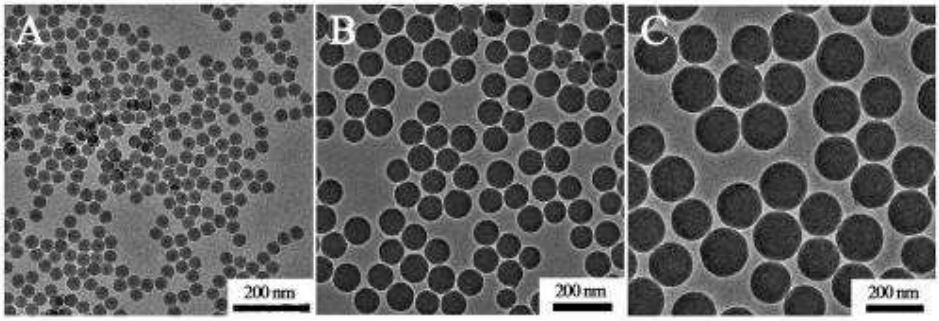

Figure S1. TEM images of the dense SiO_2 spherical nanoparticles as an initial seed with different sizes. It can be seen that the obtained dense SiO_2 spherical nanoparticles are very uniform. The size of the dense SiO_2 nanospheres can be well controlled from 30 ~ 170 nm.

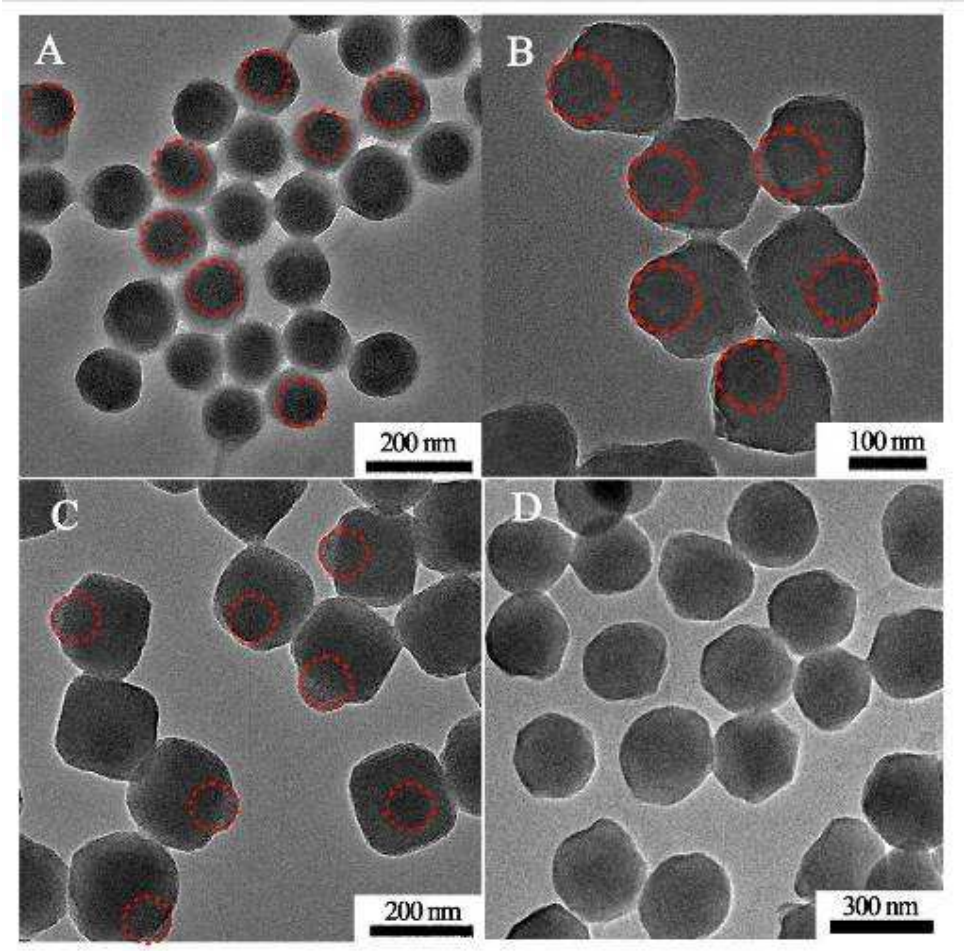

Figure S2. TEM images of the morphology evolution of the eccentric nanocomposites: from Janus to eccentric core@shell structure. As the reaction prolongs, the dense SiO_2 spherical nanoparticles were continuously wrapped by PMOs, the exposed portion of dense SiO_2 nanospheres was gradually decreased until disappeared.

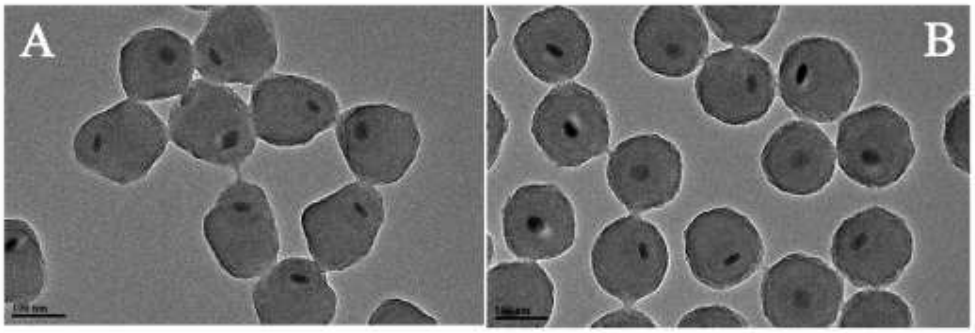

Figure S3. TEM images of the Janus UCNP@SiO_2&PMO (UCNP = upconversion nanoparticle) (A), and eccentric UCNP@SiO_2@PMO core@shell nanocomposites (B). It can be seen that the obtained nanocomposites are very uniform. As the reaction prolongs, the Janus UCNP@SiO_2&PMO nanocomposites can be evolved into eccentric UCNP@SiO_2@PMO core@shell nanocomposites.

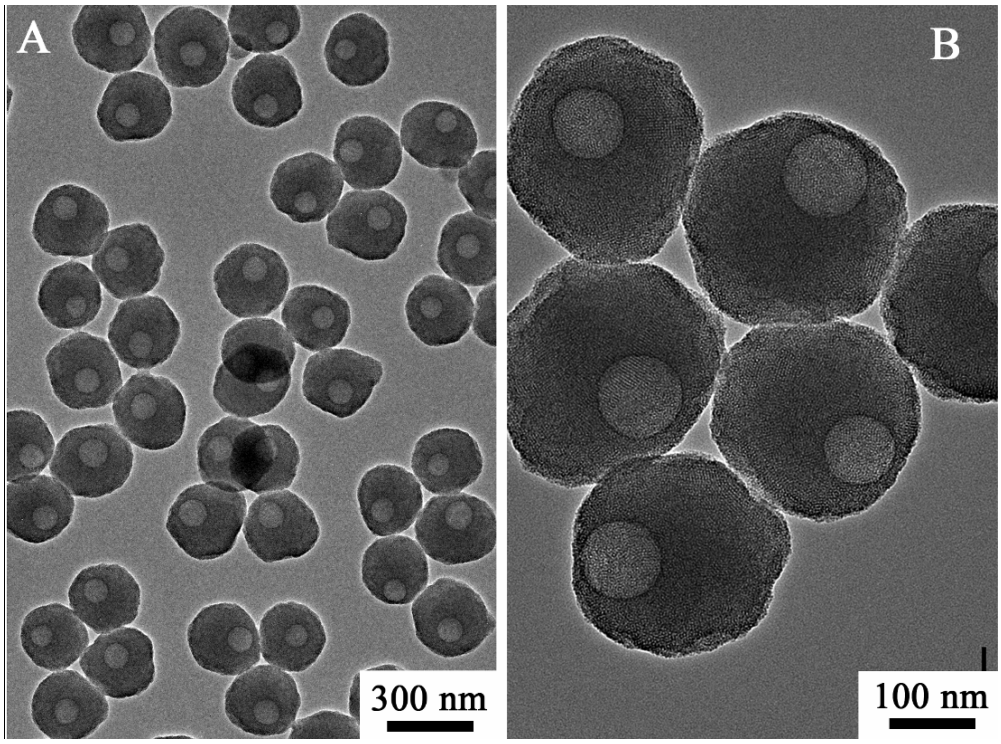

Figure S4. TEM images of the eccentric hollow PMO nanoparticles at low (A) and high (B) magnifications. It can be seen that the dense SiO_2 spherical nanoparticles can be etched to form the eccentric hollow PMO nanoparticles after the post-hydrothermal treatment at 60 °C. The hollow PMO nanoparticle shells consist of the mixed ordered mesoporous and disordered mesoporous structures.

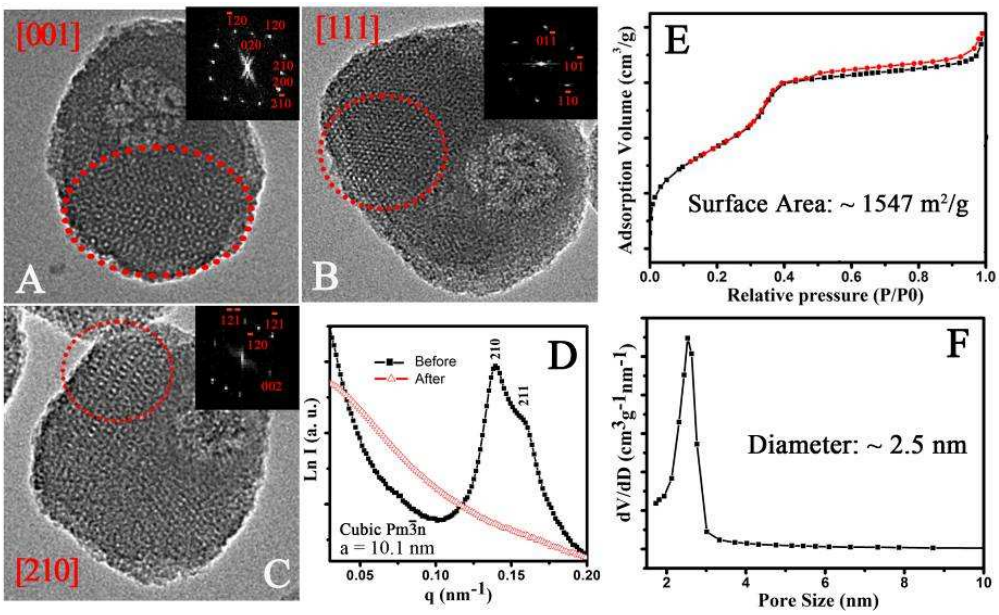

Figure S5. (A-C) TEM images and the corresponding fast Fourier transform of the eccentric hollow structure nanoparticles (before HF etching) along [001] (A), [111] (B), and [210] (C) zone axis. (D) SAXS patterns of the eccentric hollow structure nanoparticles before and after HF etching. (E, F) N_2 sorption isotherms and the pore size distribution of the eccentric hollow structure nanoparticles before HF etching. N_2 sorption isotherms show typical type-IV curves with a rapid increase in the adsorption branch at a relative pressure of 0.2 – 0.4, clearly indicating uniform mesopores. From the pore size distribution curve obtained by the Barrett-Joyner-Halenda (BJH) method, it is found that the eccentric hollow structured nanoparticles (before HF etching) exhibit a rather narrow mesopore size distribution with an average diameter of ~ 2.5 nm.

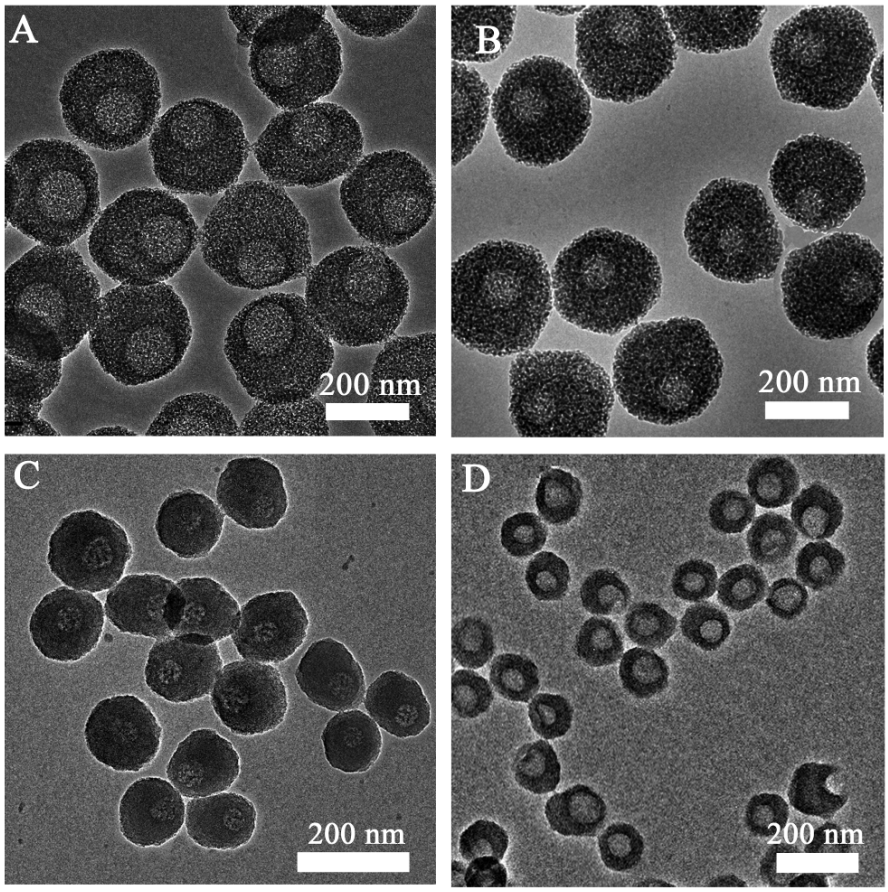

Figure S6. TEM images of the single-hole mesoporous nanocages with different particle size (A, 240 nm; B, 240 nm; C, 130 nm; D, 100 nm) and hollow size (A, 170 nm; B, 65 nm; C, 50 nm; D, 35 nm). It can be seen that the diameter and hollow cavity of the single-hole mesoporous nanocages can be well controlled at 100 ~ 240 nm and 35 ~ 170 nm by tuning the amount of the organic silane precursor and the size of the dense SiO_2 nanosphere seeds.

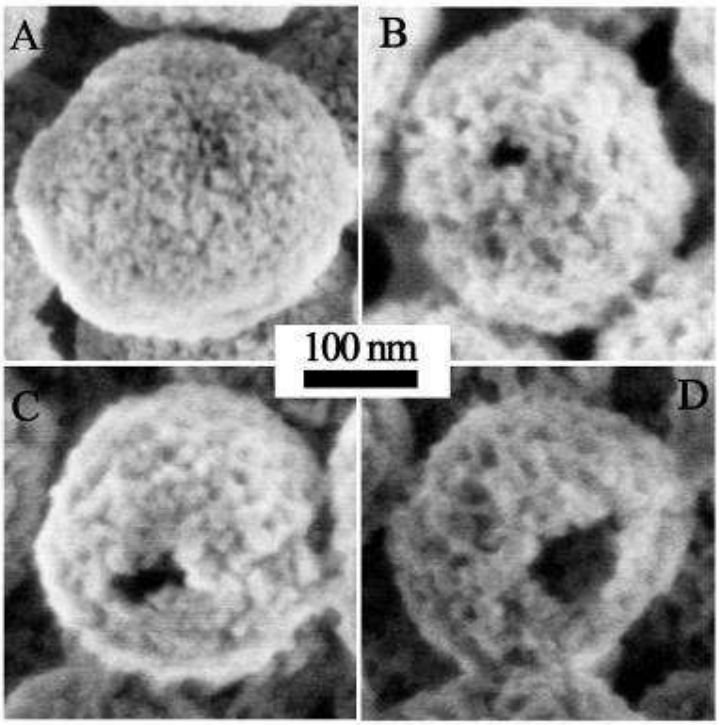

Figure S7. Typical SEM images of the single-hole mesoporous nanocages with different hole sizes in the shells by controlling HF (0.2 %) etching time: (A) 3 min, (B) 5 min, (C) 10 min, (D) 30 min. It can be seen that the asymmetric hollow structures are retained, and the hole size is increased as the etching time.

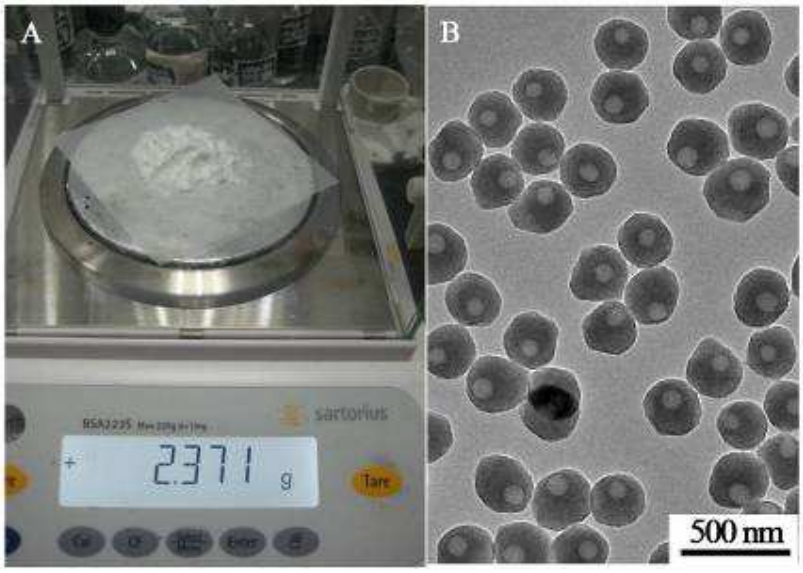

Figure S8. Gram-scale synthesis of the eccentric-hollow-structured nanoparticles before HF etching, showing that the preparation can be scaled up, gram-scale production can be realized in one reaction batch.

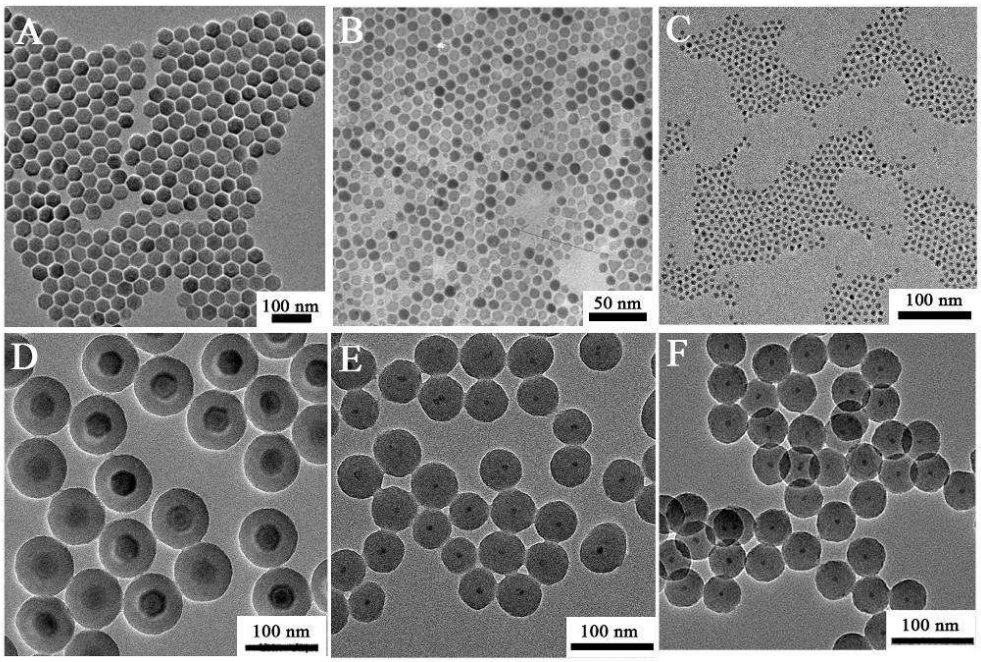

Figure S9. (A-C) TEM images of the obtained inorganic nanocrystals: (A) $NaGdF_4$:Yb,Tm@$NaGdF_4$ upconversion nanoparticles (UCNPs), (B) Fe_3O_4 nanoparticles, (C) CdSe@CdS@ZnS quantum dots (QDs); (D-F) TEM images of the obtained the obtained (D) UCNPs@SiO_2, (E) Fe_3O_4@SiO_2, (F) QDs@SiO_2 core@shell nanoparticles.

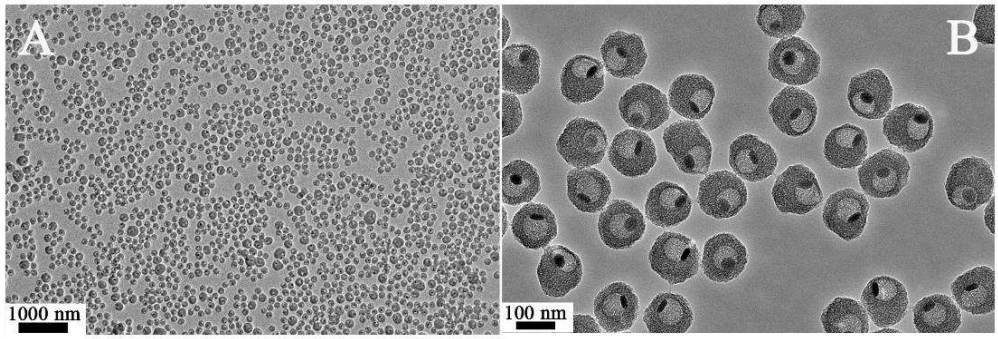

Figure S10. TEM images of the obtained single-hole UCNP@MSN nanorattles (UCNP = upconversion nanoparticles; MSN = mesoporous silica nanoparticles) at low (A) and high (B) magnifications. It can be seen that the obtained single-hole nanorattles have a uniform sphere shape with an average diameter of ~ 150 nm. The nanospheres retain the morphology of the eccentric hollow structure with a single hole on the surface of the shells and an upconversion nanoparticle in the hollow.

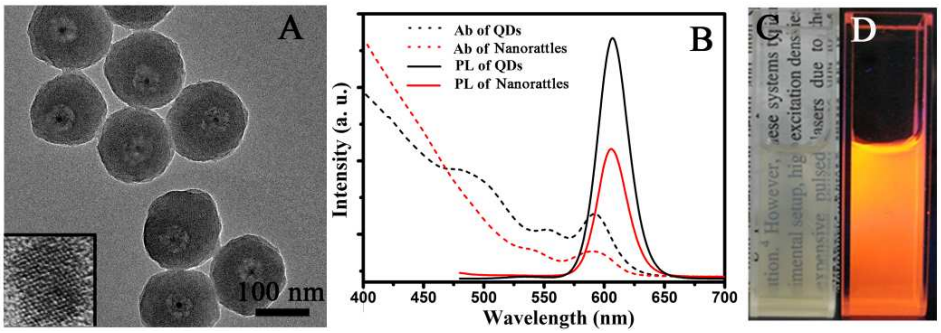

Figure S11. (A) TEM image of the obtained eccentric QD@MSN (QD = quantum dot; MSN = mesoporous silica nanoparticle) nanorattles (before HF etching). Inset: typical HRTEM image of the CdSe@CdS@ZnS quantum dots in the nanorattles. (B) The UV-Vis absorption and photo luminescence spectra of the bare CdSe@CdS@ZnS quantum dots and eccentric QD@MSN nanorattles (before HF etching). (C, D) Optical photographs of the eccentric QD@MSN nanorattles under daylight (C) and UV light at 365 nm (D). It is shown that the eccentric nanocarriers can also be endowed downconversion luminescence. Note: because CdSe@CdS@ZnS quantum dots can be corroded by HF, the results shown in this figure are not undergone the HF etching step.

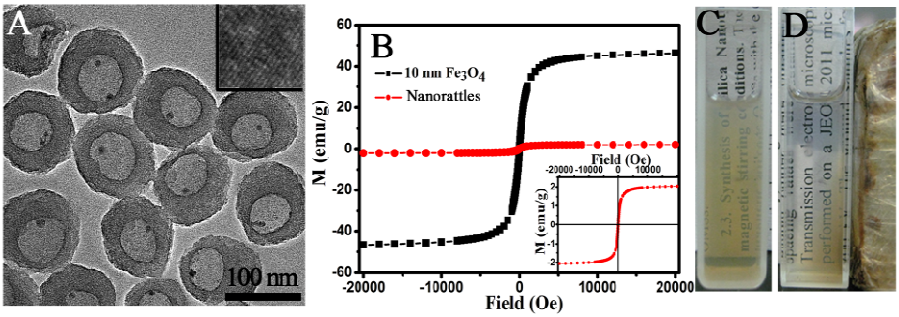

Figure S12. (A) TEM image of the obtained eccentric Fe_3O_4@MSN (MSN = mesoporous silica nanoparticle) nanorattles (before HF etching). Inset: typical HRTEM image of the Fe_3O_4 single nanoparticle in the nanorattles. (B) The hysteresis loops of the bare Fe_3O_4 nanoparticles and eccentric Fe_3O_4@MSN nanorattles (before HF etching). (C, D) Optical photographs of the eccentric Fe_3O_4@MSN nanorattles solution before (C) and after (D) the addition of magnetic field (D). It is shown that the eccentric nanocarriers can also be endowed magnetic property by using Fe_3O_4@SiO_2 core@shell nanoparticles as the initial seed. Note: because Fe_3O_4 nanoparticles can be corroded by HF, the results shown in this figure are not undergone the HF etching step.

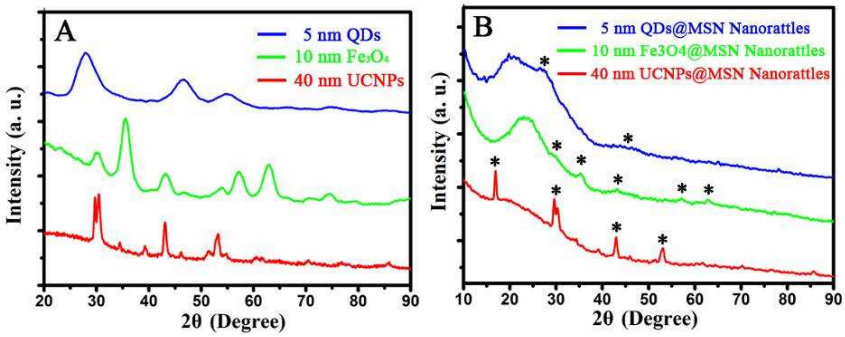

Figure S13. (A) XRD patterns of the bare $NaGdF_4$:Yb,Tm@$NaGdF_4$ upconversion nanoparticles (UCNPs), Fe_3O_4 nanoparticles, and CdSe@CdS@ZnS quantum dots (QDs). (B) XRD patterns of the obtained eccentric UCNP@MSN, Fe_3O_4@MSN, QDs@MSN (MSN = mesoporous silica nanoparticle) nanorattles.

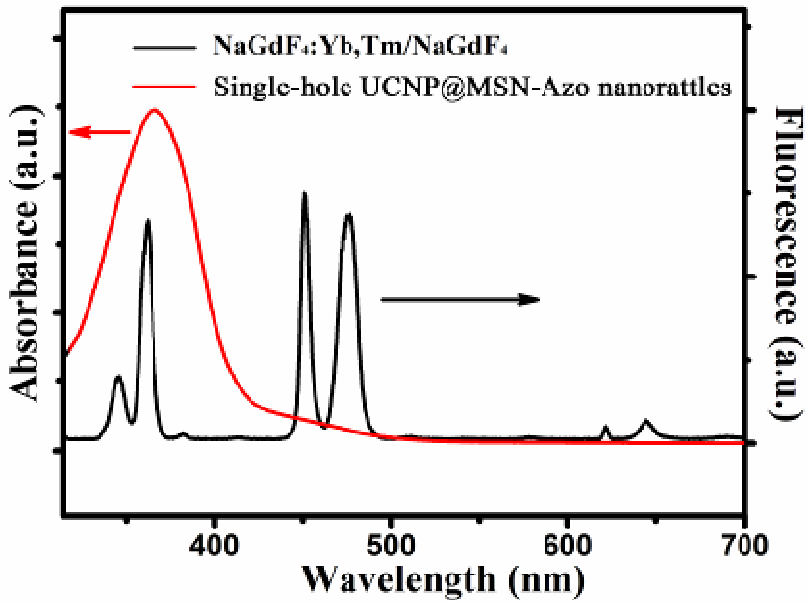

Figure S14. UV-Vis absorption spectra of the Azo-modified single-hole UCNP@MSN (UCNP = upconversion nanoparticles; MSN = mesoporous silica nanoparticle) nanorattles and the upconversion luminescence spectra of the β-$NaGdF_4$:Yb,Tm@$NaGdF_4$ upconversion nanoparticles. It can be seen that the absorption of the Azo-modified single-hole UCNP@MSN nanorattles matches well with the upconversion luminescence spectra of the upconversion nanocores, indicating that the UV/Vis light emitted by the UCNP cores can be absorbed immediately by the photo-responsive Azo molecules in the mesopore frameworks of the single-hole nanorattles.

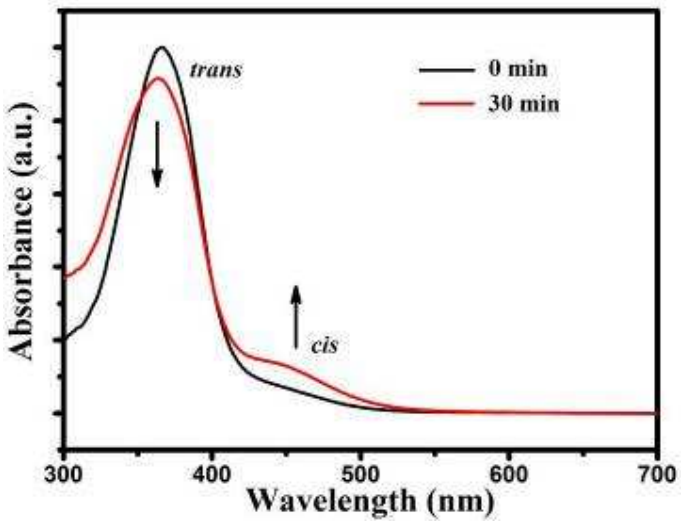

Figure S15. UV-Vis absorption spectra of the Azo-modified single-hole UCNP@MSN (UCNP = upconversion nanoparticles; MSN = mesoporous silica nanoparticle) nanorattles after the 980-nm NIR laser irradiation for 0 min and 30 min. NIR light exposure intensity was 5 W/cm^2. It can be seen that with the increase of NIR irradiation duration, the absorbance of the maximal absorption band of the Azo moiety at 355 nm decreases apparently. In contrast, the absorption band of the Azo moiety at 450 nm increases slightly, indicating that the UV and visible light from UCNPs causes the *trans-cis* photoisomerization of the Azo molecules in the mesopore frameworks of the single-hole nanorattles.

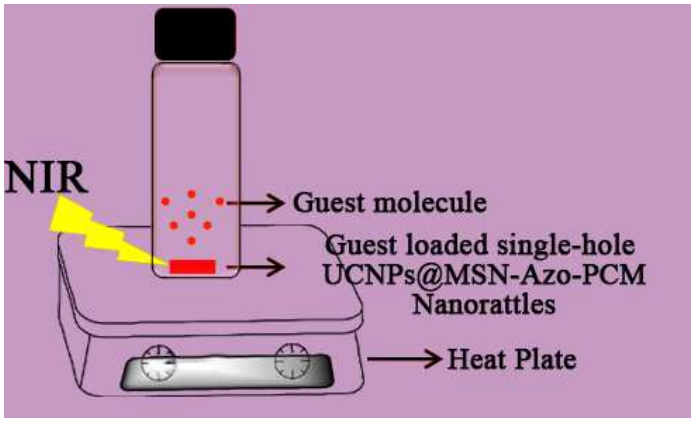

Figure S16. Schematic illustration of heat and NIR upconversion bimodal triggered guest release experiments.

Table S1. The BET surface area, pore sizes and adsorption capacities of the control samples: mesoporous silica ($mSiO_2$), pure PMO, hollow structured PMO, and the single-hole PMO nanocages.

	Surface Area (m^2/g)	Pore Size (nm)	DOX Adsorption Capacities (mg/g)	BSA Adsorption Capacities (mg/g)
$mSiO_2$[a]	800	2.4	67	153
PMO[a]	1520	2.4	43	98
Hollow PMO[a]	1100	2.2	52	141
Single-hole PMO nanocages	494	3 ~ 30	33.6	342

[a] The syntheses of $mSiO_2$, pure PMO and hollow PMO were similar to our previous report.[8]

It can be seen that the mesoporous silica ($mSiO_2$, synthesized by using TEOS) exhibits the highest loading capacity for the small sized guest (DOX, doxorubicin hydrochloride) due to its hydrophilcity of the mesopore channels. Because of the difference in BET surface area, both the pure PMO and hollow structured PMO samples show higher loading capacity than the single-hole PMO nanocages. For the loading capacity for bigger guest molecule (BSA), the $mSiO_2$, pure PMO, and hollow structured PMO all exhibit lower loading capacities compared with the single-hole PMO nanocages, because the formers have the smaller mesopore channels.

References

[1] Li, X.; Shen, D.; Yang, J.; Yao, C.; Che, R.; Zhang, F.; Zhao, D. Y. *Chem. Mater.* **2013**, *25,* 106.

[2] Zhou, C.; Yuan, H.; Shen, H.; Guo, Y.; Li, X.; Liu, D.; Xu, L.; Ma, L.; Li, L. S. *J. Mater. Chem.* **2011**, *21,* 7393.

[3] Li, X.; Si, H.; Niu, J. Z.; Shen, H.; Zhou, C.; Yuan, H.; Wang, H.; Ma, L.; Li, L. S. *Dalton Trans.* **2010**, *39,* 10984.

[4] Lu, J.; Choi, E.; Tamanoi, F.; Zink, J. I. *small* **2008**, *4*, 421.

[5] Peng, Z.; Yang, H. *Nano Today* **2009**, *4*, 143-164.

[6] Goebl, J. A.; Black, R. W.; Puthussery, J.; Giblin, J.; Kosel, T. H.; Kuno, M. *J. Am. Chem. Soc.* **2008**, *130*, 14822-14833.

[7] Carbone, L.; Cozzoli, P. D. *Nano Today* **2010**, *5*, 449-493.

[8] Li, X.; Zhou, L.; Wei, Y.; El-Toni, A. M.; Zhang, F.; Zhao, D. Y. *J. Am. Chem. Soc.*

2014, *136*, 15086.